Proceedings World Geothermal Congress 2010
Bali, Indonesia, 25-29 April 2010

Stress Heterogeneity in the Granite of the Soultz EGS Reservoir Inferred from Analysis of Wellbore Failure

Benoît Valley*,** and Keith F. Evans*

* Engineering Geology, Swiss Federal Institute of Technology (ETH), CH-8092 Zürich, Switzerland; **now: MIRARCO Mining Innovation/Laurentian University, 935 Ramsey Lake Road, Sudbury, ON P3E 2C6, CANADA

bvalley@mirarco.org, keith.evans@ethz.ch

Keywords: Borehole failure, Stress characterisation, Stress heterogeneities, Rhine Graben, Enhanced Geothermal System, Soultz-sous-Forêt

ABSTRACT

Stress heterogeneity is thought to play an important role in many aspects of crustal mechanics, including the influencing of the space-time distribution and scaling of earthquakes. As such, it is likely to have some influence on the reaction of rock masses to massive fluid injection such as at EGS sites. Unfortunately, too little is known about the magnitudes of spatial variations of stress in the crust, primarily because heterogeneity is so difficult to measure. In this paper we describe variations in stress orientation indicated by wellbore failure in two boreholes of the Soultz-sous-Forêts EGS site and attempt to explain them. A novel feature of these data is that the holes are separated by only 20 m between 1400 m and 2400 m where DITFs cover 55% of the borehole lengths, thus allowing the lateral coherence of the variations to be examined.

The variations are seen to occur at all scales, from relatively abrupt changes over a couple of metres, to gradual variations over scales of several hundred metres. Deviations in SHmax orientation from the mean in excess of 90° occasionally occur. The variations follow a power law scaling with an index close to -2.0, indicating self-affine behaviour where variations appear progressively "rougher" at shorter scales. Two large long-wavelength (>100 m) variations seen at 2.0 and 4.7 km correlate with the two most prominent fracture zones penetrated by the wells. The lowermost stress perturbation extends over several hundred metres and is characterised by SHmax rotations of up to 90° and changes in the mode of failure from compression (breakouts) to tension (DITFs). The uppermost stress perturbation occurs where the wells are separated by only 20 m, and is only partly correlated between wells, indicating high spatial gradients in stress about the perturbing fracture zone. Short wavelength variations in orientation occur more or less continuously and are usually associated with natural fractures. Little coherence is seen for short-wavelength variations between wells. Almost all fractures associated with stress perturbations are "critically stressed" under the linear stress characterisation of the site. E-DITFs are often seen to form parallel to natural fractures, which typically dip at 50 – 70°. The parallel geometry suggests partial relaxation of shear stress from near critical level on the associated natural fractures.

1. INTRODUCTION

Analysis of stress induced wellbore failure is a powerful tool to characterise the state of stress (e.g. Bell and Gough, 1979; Zoback et al., 2003). In rocks without strong strength anisotropy, the failure is controlled by the variation in tangent stress that develops around the wellbore circumference when the maximum stresses in the plane normal to the wellbore are not equal. Failure may be compressional where the tangent stresses reach a maximum, producing breakouts, or tensile where they reach a minimum, giving rise to so-called drilling-induced tension fractures (hereafter referred to as DITFs). Wellbore failure occurs in the 5 km deep wells at Soultz-sous-Forêts (see Figure 1 for location), with DITFs dominating above 3 km and breakouts below 3.5 km. The data have been analysed by Valley and Evans (2007) to obtain the linear depth trends of the attributes of the stress tensor at Soultz, as needed for site stress characterisation. That study ignored the small and medium scale deviations from the large-scale trends. Such perturbations are commonly called stress heterogeneities, and they are believed to play a significant role in earthquake complexity (e.g. Shaw, 2004; Zöller et al., 2005), faulting mechanism (e.g. Faulkner et al., 2006), errors in the stress estimates obtained from inversion of earthquake focal mechanism (e.g. Cornet and Jianmin, 1995; Cuenot et al., 2006; Scotti and Cornet, 1994) and reservoir stimulation (e.g. Cornet et al., 1992).

Despite their perceived importance, stress heterogeneities are difficult to reliably identify, let alone quantify. Stress-induced wellbore failure in deep holes offers perhaps the best opportunity to study the spatial variability of stress. In this paper we present results of an analysis of deviations for the linear stress trends in the Soultz wells to 5 km as expressed through the breakouts and DITFs. A novel aspect of the data is that the two wells that serve as the data source are separated by only 15–30 m over the depth range 1.5–2.5 km. Thus, the lateral variation of the stress perturbations as well as the vertical can be examined. Possible stress perturbing mechanisms which may explain these variations are discussed.

2. BACKGROUND

The effect of gravity is such that stress magnitudes usually increase with depth. Commonly, the increase at a particular locality is seen to be reasonably well approximated by linear trends for the magnitude of the two horizontal and the vertical principal stresses, the latter being equal to the integrated overburden, and a constant orientation for the horizontal principal stresses. This description is referred to as the linear stress characterisation of a site. Valley (2007) has presented a linear characterisation for the Soultz-sous-Forêts geothermal site. In this paper, stress variations or perturbations shall be taken to mean deviations in stress from this simple linear description.

There is good reason to believe that stress variations should occur on all scales The perturbation of stress around faults that slip in earthquakes is demonstrated by the success of the Coulomb stress concept in predicting aftershock distributions (Harris, 1998). This perturbation occurs on scales of the order of the length of slip, and so, since

earthquakes occur on all scales, perturbations of stress can be expected on all scales. However, the magnitude of the variations in stress that can build up as a consequence of the repeated action of stress-perturbing mechanisms is tempered by the limited strength of the fractured and faulted crust. For example, a stress perturbation generated by slip on a fault can be partly relaxed by post-seismic slip on secondary fractures and faults, of which aftershocks are a manifestation. Thus, the processes at work are complicated, and our understanding of the degree of stress variability that typically prevails within the crust (if one can generalise), is poor.

The limited state of knowledge has important implications for the development of EGS projects, because it bears on the issue of whether the state of stress at a prospective EGS site will be essentially the same as at a site say ten kilometres distant where stress has been characterised. In this regard it is important to note that the approximately N–S mean orientation of maximal horizontal principal stress at Soultz is significantly different to the regional orientation of NW–SE. It is thus relevant to quantify the deviations in the state of stress from the simple linear characterisation, and understand their origin. Another implication is related to the modelling and prediction of stimulation processes. Indeed, one basic input for most if not all numerical simulations of reservoirs is the initial state of stress. The uniform state of stress provided by the linear site characterisation reflects only partially the actual in-situ conditions. The introduction of stress heterogeneities into the initial stress conditions of the models would bring the simulations closer to reality and thus may give some improvement of the quality of the model predictions. This is particularly true for models that seek to simulate induced micro-earthquake frequency-moment distributions.

3. PRESENTATION OF THE DATA

The data analysed in this study stem from two of the three deep boreholes drilled to 5km in granite at the Soultz-sous-Forêts geothermal project site where the granite top lies at 1400 m (Figure 1). The main sources of information are UBI (ultrasonic borehole imager) images collected in these boreholes.

The UBI data were acquired in two holes GPK3 and GPK4 which were drilled from the same pad. Both are sub-vertical in the upper 2–3 km, and penetrate granite at 1.4 km, which means their separation in the uppermost kilometre of granite to 2.4 km is less than 20 m (Figure 2b). Below 2.5 km, the wells deviate from vertical to build up separation before returning to sub-vertical in the lowermost 500 m (Figure 2a). The granite sections in both wells were drilled with a 12-1/4 inch bit to 4514 m TVD (GPK3) and 4489 m TVD (GPK4), and then with 8-1/2 inch to total depth. The UBI logs in each well were run after completing each section, about a month apart. The wells were drilled one year apart. The same UBI sonde was used for both sections of each well but different sondes were used for each well.

Wellbore failure was identified from both the travel-time (i.e. borehole geometry) and acoustic reflectivity images. Breakouts are typically manifest as pairs of diametrically-opposite spall zones that extend along the borehole axis. They occur where the maximum tangent stress acting at the borehole wall exceeds the compressive strength of the rock. In the simple case of a vertical borehole penetrating a rock mass in which one principal stress is vertical, this maximum occurs in the direction of the minimum horizontal principal stress, Shmin (Bell and Gough, 1979).

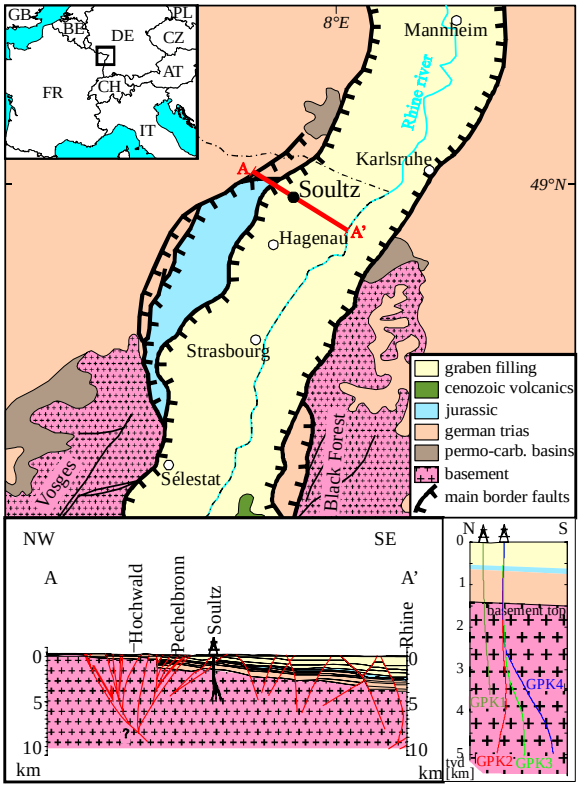

Figure 1: Soultz-sous-Forêts is located within the Upper Rhine Graben in north-eastern France. The Upper Rhine Graben is a Cenozoic structure part of the West European Rift System. The Soultz wells penetrate about 1.4 km of Cenozoic and Mesosoic sediments before entering the granitic basement rocks.

DITFs are identified primarily on acoustic reflectivity images where they show as thin, often ragged fracture traces that may be either axial or en-echelon. DITFs seen on UBI images from the 3.6 km deep well GPK1 do not show on Azimuthal Resistivity Imager (ARI) logs, indicating they do no penetrate deeply. DITFs occur when the tangent stress at the borehole wall becomes sufficiently tensile to produce tensile failure. Although, in principle, the minimum tangent stress produced by far-field stresses can be tensile, it is usually the cooling stress component arising from the circulation of cool drilling fluids that is decisive in driving the minimum tangent stress to negative values and producing tensile fracturing. However, the cooling stress is axi-symmetric, and so the location of the tensile fracture is governed by the far-field principal stress orientations. In the case of a vertical borehole penetrating a medium in which one principal stress is also vertical, the least compressive tangent stress at the borehole wall is horizontal and occurs in the direction of SHmax. This results in a pair of diametrically-opposite DITFs, which hereafter are denoted by A-DITFs. However, if the borehole axis is not aligned with a principal axis and the criterion for tensile failure is met, the least compressive tangent stress at the borehole wall will in general be inclined to the borehole circumference. In this case, tensile failure will occur as a stack of slightly-overlapping en-echelon tensile fractures, which hereafter are denoted by E-DITFs. The relationship between the induced fracture geometry and the in-situ stress attributes (i.e. orientations and magnitudes) in this case is not as simple as in the aligned case (e.g. Peška and Zoback, 1995).

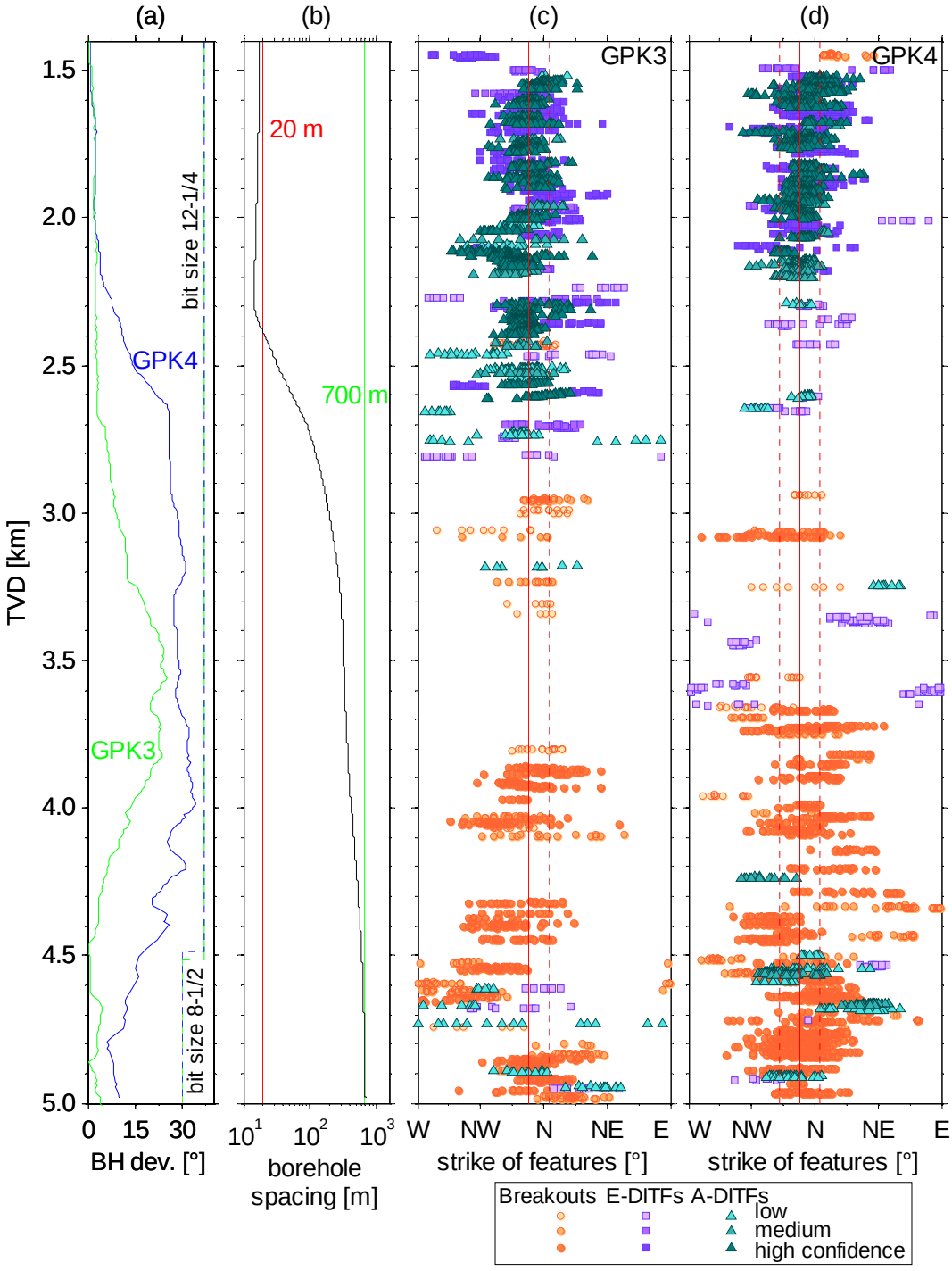

Figure 2: a) boreholes deviation from vertical and bit size (green GPK3 and blue GPK4). b) horizontal separation of the boreholes plotted on a logarithmic scale. c) and d) strike of A-DITFs (green triangles), E-DITFs(violet squares) and breakouts (orange circles) with the latter rotated anticlockwise through 90 for GPK3 and GPK4 respectively. The mean azimuth of SHmax and its standard deviation from all indicators in both GPK3 and GPK4 is denoted by the vertical redlines (N169°±14°).

The procedure employed in this study for describing the wellbore failure observations is as follows. First, intervals affected by breakouts, A-DITFs, or E-DITFs were identified. Then, for breakouts and A-DITFs, the mean azimuth of the two limbs of the features was determined for successive 0.5 m depth windows. For E-DITFs, the best-fitting plane to each member of each fracture pair was found and the strike and dip of the plane noted. Typically, this led to one sample every 0.5 to 1.0 m. In all cases, the confidence of the identification was quantified by assigning an index ranging between 1 and 3, corresponding to low and high confidence respectively.

4. VARIABILITY OF STRESS INDUCED FAILURE ORIENTATION

4.1 General Variability in the Orientation of Stress Indicators

The orientation distributions of high confidence breakouts and DITFs in each borehole are shown in Figure 3. The stereographic plot of poles of the true orientation, i.e.

corrected for borehole deviation, of DITFs indicates a wide range of fracture strikes, although the rose diagram of Figure 3b makes clear that the vast majority of DITFs lie within 20° of the mean orientation with outliers being relatively few in number. A 5° discrepancy in mean orientation of the DITFs in the two boreholes is evident, and a 10° discrepancy in the same sense for breakouts (Figure 3c). Given that the horizontal distance between boreholes is less than 35 m for the section where most of the DITFs occur (1400 m to 2500 m depth), so that essentially the same rock volume is sampled, the discrepancy must be due either to stress variations occurring over relatively short horizontal distances or to some systematic error in the logging process. The former explanation seems improbable, given that the observations span a depth range of 3.5 km. The UBI logs are oriented by coupling the sonde to a GPIT (General Purpose Inclinometer Tool) sonde. Different GPIT sondes were used in GPK3 and GPK4, but the same sonde was used for both sections of each well. Thus, calibration error is a possible explanation.

The modal peaks of the breakout distributions, which are shown in Figure 3c rotated through 90° to permit direct comparison with the DITFs, are essentially identical to the means of the DITF populations for the same hole. The distributions of the strikes of breakouts show greater scatter than the DITFs. This is at least partly due to the angular width that breakouts span which makes the determination of their representative orientation more uncertain than for DITFs. A slight asymmetry of the breakout distribution is also visible for each borehole but particularly for GPK3 data: the distribution is slightly overbalanced in an anti-clockwise sense about the mode of the distribution, which is approximately aligned with the DITFs strike directions. This may reflect a bimodal distribution with a main mode at 168° and a weak secondary mode at about 150°. Such a deviation may be associated with the reported counter-clockwise bias in the orientation distribution of hydro-thermally altered shear structures compared to the mean orientation of all fractures (Evans et al., 2005, Fig. 3). The same explanation was used by Bérard (2003) (see also Cornet et al., 2007, Fig. 5) to interpret a bimodal distribution seen in the orientation of wellbore failure in GPK2, although in that case the described features were ‘thermal breakouts’ — borehole elongation in the SHmax direction — a proposed new type of wellbore failure.

With very few exceptions, deviations from verticality of E-DITFs are less than 30° (Figure 3a). Some deviation from verticality of the DITFs are expected in inclined borehole sections even if one principal stress was always exactly vertical. The exact amount of deviation from verticality of the DITFs in such cases depends on the borehole deviation, the stress ratios and the Poisson ratio of the rock (e.g. Peška & Zoback, 1995). In the conditions encountered at Soultz, such deviations should not exceed about 10°. Thus, occasional deviation from verticality of a principal stress direction has to be assumed in order to explain the observed DITFs orientation pattern. Non-vertical DITFs dip preferentially to the east. In that respect, they mimic natural fractures which show similar preference in the upper section of the wells (Dezayes et al., 2010). A-DITFs and E-DITFs are clearly distinguished in Figure 3a, the former lying around the margin of the stereoplot, and the latter lying inside. E-DITFs with small deviation from axial are rare or absent, indicating that a critical deviation of the ‘vertical’ principal stress from alignment with the borehole axis is required before DITFs form in the en-echelon mode. This behaviour has been predicted theoretically (Ito et al., 2001). Neighbouring tensile fractures developing only a few degrees out of alignment with the borehole axis will tend to interact and link to form an axial fracture, albeit a ragged one. At some misalignment, the interaction will be insufficient for linkage to occur, resulting in en-echelon fractures.

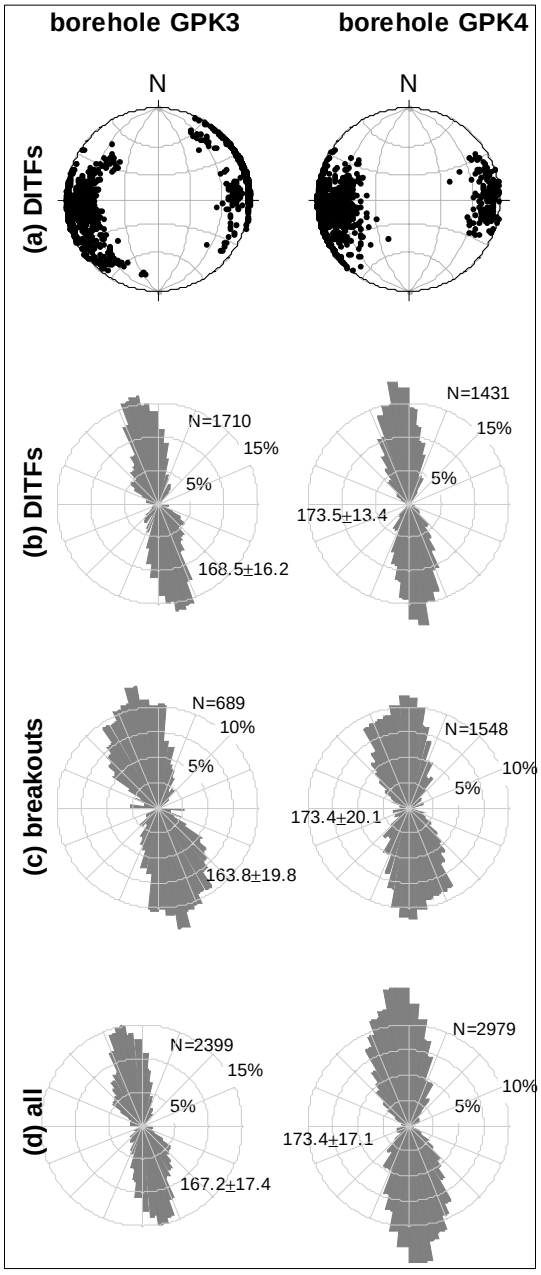

Figure 3: Orientation of high confidence stress induced wellbore failure in GPK3 and GPK4. Data from entire borehole length including both sub-vertical and inclined sections are shown. a) Stereographic plot of poles to DITF planes (equal area, lower hemisphere). b) Distribution of strikes of DITFs. c) Distribution of the orientation of borehole breakouts rotated through 90° to facilitate direct comparison with the DITFs. d) strike orientation of all features together. Here also, 90° has been added to the breakouts directions. For all circular histograms, N is the number of data point and the circular mean and single standard deviation are also displayed.

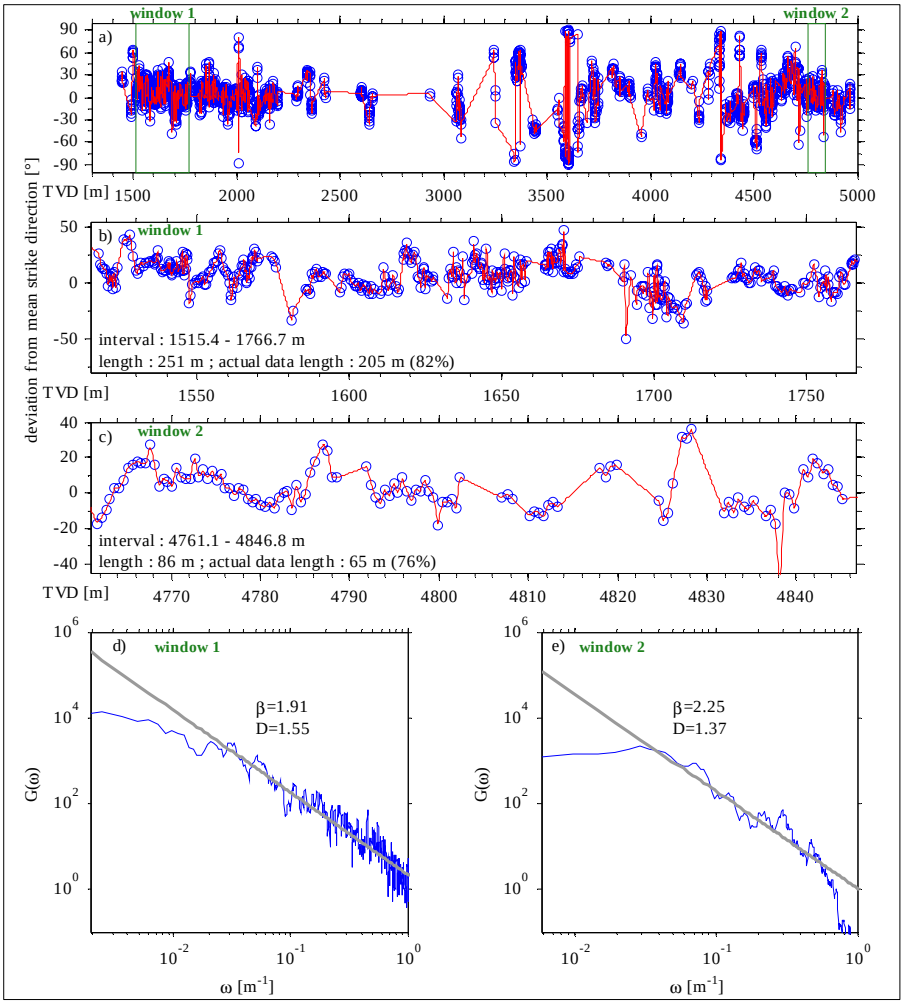

Figure 4: Power spectral analysis of the stress orientation variations in GPK4. a) Variation about the mean for the entire borehole. The blue circles denote data, and the red line is the linear interpolation of the data. The data sections used in the analysis are indicated. b) expanded view of the data window near the upper part of the borehole where DITFs occur. c) expanded view of the data window near the lower part of the borehole where breakouts occur. d) power spectrum of the data shown in b). The slope, β of the high-frequency roll-off and the fractal dimension, D, are indicated. e) power spectrum of the data shown in c).

4.2 Variability with Depth of the Stress Orientation Indicators

The depth profiles of the orientation of breakouts and DITFs are shown in Figure 2c and 2d for GPK3 and GPK4 respectively. DITFs occur almost exclusively above 3.0 km, whereas only breakouts are confidently identified below 3.7 km. This partitioning of the different modes of failure reflects the depth trends of stress magnitude, as discussed by Valley and Evans (2007). Here we are interested only in the variation in the orientation of the horizontal principal stresses that the two indicators imply. The variation of the orientations of the breakouts and DITFs about the mean for the site is shown in Figures 4a for GPK4. The nature of the variations is made clearer in the expanded views over selected depth windows in Figures 4b and 4c. Evidently, depth sections where the indicators have a stable orientation are rare: in most cases, the continuous sections of breakouts or DITFs show locally-progressive rotation in one direction or the other. These local rotations appear as streaks in the compressed-depth profiles in Figures 2c and 2d.

The variations occur at all scales. This is demonstrated in Figure 4d/e where the power spectral density, $G(\omega)$, of the variations in breakout- or DITF-orientation over the depth windows are shown. The windows were chosen to correspond to depth sections with relatively continuous data so as to reduce the bias introduced by gap-filling. The inevitable gaps were filled with linear interpolations and the series resampled with constant spacing. The spectra were computed using the periodogram method (e.g. Stoica and Moses, 1997) and the resulting spectra smoothed with a 5 point moving-average filter. Results are shown on log-log plots for the full range of spatial frequencies obtained from the analysis (i.e. from the highest, the Nyquist, down to the lowest, the reciprocal of the total window length).

It is evident that at high spatial frequencies, the spectral decay conforms relatively closely with a linear trend of slope, β, indicating that the orientation variations follow a power law of the type $G(\omega) \sim \omega^{-\beta}$. The slopes, β, of the linear 'roll-offs' were determined by least-square fitting over the appropriate frequency band, ignoring deviations from linearity in the spectra extremities, and found to be close to 2.0 for both GPK4 (Figure 4) and GPK3 (Valley, 2007). Power laws with slopes greater than -3.0 (e.g. -2.0) indicate a fractal process, the fractal dimension, D, being given by $D = (5-\beta)/2$ (Power and Tullis, 1991; Turcotte, 1989). A slope of -3.0 indicates self-similarity (i.e. scale invariance). Orientation variations that follow a power law with a slope of -3.0 would thus look identical at all scales

(Power and Tullis, 1991). Slopes greater than -3.0 indicate self-affine behaviour, where variations look progressively rougher at smaller scales. The proportionate reduction with increasing wavelength of the magnitude of the variations relative to wavelength as expressed by the self-affine scaling laws is expected for directional data where the maximum deviation is limited at 90°. These power laws hold for wavelengths from 4 m up to 80 m, the longest wavelength that could be resolved from the short data spans. So it is clear that variations in horizontal principal stress orientation occur at various scales.

In the following, the variations that occur at long and short wavelengths will be examined in more detail. Long wavelength variations are taken to be those that are coherent at scales larger than 50 m. Since this is larger than the spacing between the wells between 1.5 and 2.5 km, where DITFs dominate, such variations seen in the vertical profiles of stress orientation should be relatively coherent between wells, assuming that their lateral extent is similar to their vertical.

4.3 Large Scale Variations

Long-wavelength variations in horizontal principal stress orientation can only be detected where wellbore failure occurs more or less continuously over large sections of hole. This essentially restricts the study to the uppermost 1000 m of the granite, where DITF failure occurs, and the lowermost 1.2 km, where compressional failure is frequent. Long-wavelength variations in SHmax orientation can be seen in both sections in the plots of breakouts and DITFs azimuths in Figures 2c and 2d.

4.3.1 Large Scale Stress Variations in the Lower Wells Sections

Considering the lower sections first, significant variations in breakout orientation with wavelengths of several hundred metres and deviations from the mean of several tens of degrees can be seen near the bottom of both wells (Figure 2). In GPK3, a large excursion with a wavelength of about 400 m is centred at about 4650 m and has a maximum deviation from the mean of 50° to the west if the short-wavelength variations are smoothed-out. Another deviation to the west with an amplitude of 30° occurs at 4050 m, whilst at hole bottom, the deviation is 20° to the east, both having wavelengths of ~200 m. In GPK4, the only large scale excursion is centred at 4690 m. This has a deviation of about 50° to the east, and a wavelength of about 250 m.

The 400 m wavelength deviation centred at 4650 m in GPK3 almost certainly reflects the stress perturbation associated with a major fault that is penetrated at 4697 m TVD. This fault strikes approximately N160°E and dips at 50–60° to the west (Dezayes et al., 2004; Sausse et al., 2007, Dezayes et al., 2010), and is almost certainly a structure that extends many hundreds of meters if not kilometres. If the structure dips at 60°, then it would lie within 100 m of the borehole over the ±200 m length of the stress orientation perturbation. A transition from breakouts to DITFs is seen to occur near the intersection of this structure with the well, indicating that stress magnitudes are also perturbed. A major deviation in breakout orientation is also seen in GPK4 at a similar depth, but it occurs in the opposite direction. Since the well bottoms are separated by ~650 m, there is no compelling reason to expect that the two perturbations should be associated with the same fault, although that is possible. It is noteworthy that the difference in the orientations of the breakouts in GPK3 and 4 at 4650 m TVD, two points within the reservoir 650 m apart, amounts to 80°.

Another potential contribution to the stress heterogeneity near the bottoms of the holes might arise from a lithological change from standard ‘Soultz’ porphyritic granite to a ‘two-mica’ granite that occurs near 4720 m TVD. The change is believed to reflect the interface between two separate intrusions. Stress perturbations might result from contrasts in elastic moduli. Since the elastic moduli of the two mica granite have currently not been measured, this possibility remains uncertain. In any case, the dominant factor is almost certainly the fault at 4697 m TVD in GPK3.

The preferred explanation of the large-wavelength variations is that they reflect the stress generated by slip on faults. Based on the modelling results of Shamir (1990), perturbations with long wavelengths require slip on surfaces at least as large as the variations’ wavelength, which, for the present data, implies structures that are at least 200 to 450 m in length. Such sizes correspond well with the expected lengths of fracture zones within the Soultz granite (Valley, 2007). There are many fracture zones intersected by the wells (see Dezayes et al., 2010), although none produce a perturbation as extensive as that associated with the fault in GPK3 at 4697 m TVD. In part, this may reflect the gaps in the definition of the stress field orientation in wellbore sections where there are neither breakouts nor DITFs. However, it is also probably an indication of the uncommonly large size of the 4697 m structure, which is manifest by its hydraulic (Tischner et al., 2007) and seismic (Dorbath and Charléty, 2007) properties, and its impact on drilling operations (Hettkamp et al., 2004).

4.3.2 Large Scale Variations in the Upper Wells Sections

The long-wavelength perturbations in the upper section are particularly interesting because the two wells are less than 20 m apart and thus significant coherence between the variations in the wells might be expected. Figure 5 shows the large scale trend of the DITF strike determinations for the upper section of both wells. Large scale trends were extracted by applying interpolation and a moving window (boxcar) filter of 100 m to the raw data. Interpolation points filling the data gaps were given zero weighting in the averaging, and so the effective filter length is shorter near gaps. The resulting filtered series from both GPK3 and GPK4 are shown together in Figure 5 for comparison. For the depth range between 1535 m and 2200 m, which is relatively well sampled, three sections where the two series are reasonably correlated are found. These are denoted A (1535–1621 m), C (1783–1876 m), and E (2006–2200 m). However, the orientation variations between these sections are decidedly different. These are denoted as B (1621–1783 m) and D (1876–2006 m), and are marked by the light red bands in Figure 5. In section B, the two curves deviate from each other by only 9° over 60 m length scales, which is not a major inconsistency. However, the discrepancy for section D is much larger, amounting to 23° over a 130 m length scale. This is a surprising result, and it poses the question of how such a large change in stress orientation can occur vertically over a scale of 130 m yet not extend laterally only 20 m.

The origin of the discrepancy in section D is uncertain, although a reasonable working hypothesis is that it is related to a major fracture zone that intersects the wells near this depth (indicated by the black arrows in Figure 5). This fracture zone is most certainly a major structure, perhaps of

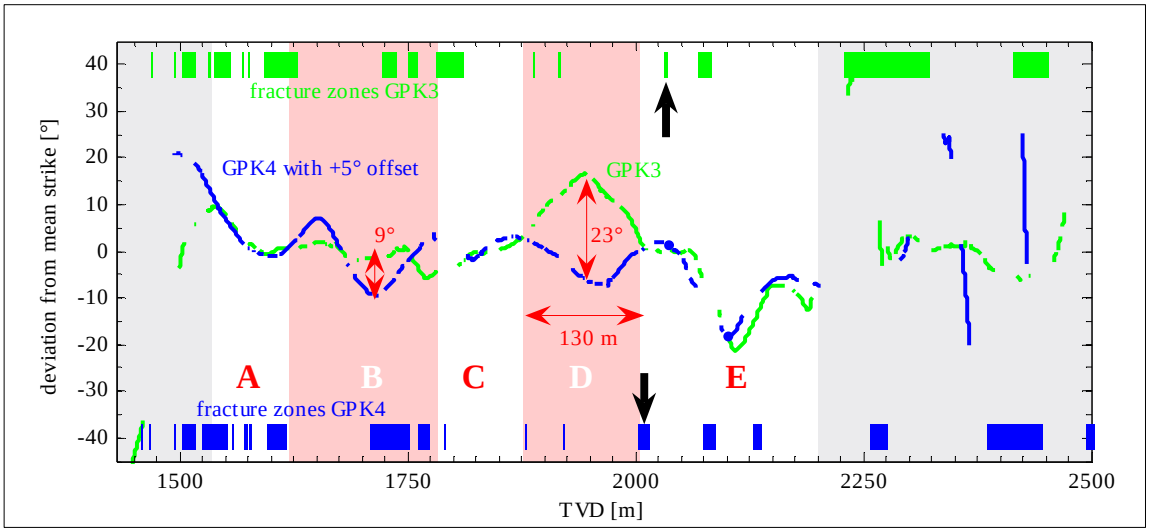

Figure 5: Superposition of the long wavelength components of the strike variations from GPK3 (green) and GPK4 (blue) extracted by interpolation in moving average filtering of the raw data. Note that the curve for GPK4 has been shifted by 5° to compensate for the apparent discrepancy in orientation measurement between the two holes. The two curves are essentially identical in zones A, C and E denoted by the white bands, but deviate significantly from each other in Zones B and D (light red bands). The distribution and width of fracture zones intersected in the two wells are shown at the top (GPK3) and bottom (GPK4) of the figure (from Valley, 2007). Black arrows point to the major fracture zone crossed by the boreholes at about 2100 m.

the same scale as the fault intersected at 4697 m TVD in GPK3 that was associated with the primary large-scale perturbation in the lower section of the reservoir. The zone was first intersected in GPK2 at 2110 m during the initial drilling of the well in 1995, and resulted in total loss of circulation fluid. No cuttings were obtained from the well during the subsequent drilling to 3876 m because they were swept into the fracture zone along with the drilling fluid. The zone was eventually plugged with 23 m^3 of cement during the extension of GPK2 to 5000 m in 1999. It is thus a zone of enormous capacity that has had a great deal of solid material injected into it. The structure dips at 74° to N95°E and crosses both wells at the bottom of the orientation discrepancy in section D (Figure 5). It is thus very close (<40 m) to the wells over the 130 m section of zone D. The discrepancy might thus reflect a particularly strong lateral gradient in stress arising from the perturbation associated with this fracture zone.

4.4 Small Scale Variations

Small-scale variations are considered to have wavelengths less than 50 m. As noted earlier, it is rare for the strike of breakouts or DITFs to remain stable over tens of metres of borehole. More commonly, they rotate systematically in one direction of another for a short distance, giving rise to the seemingly horizontal streaks in Figures 2c and 2d. An expanded view of DIFTs strike orientation in the upper section of GPK4 illustrates this case and is presented on Figure 6. Deviations from the local mean orientation of more than 45° occasionally occur (Figure 3). The variations in strike indicate that, more often than not, the azimuths of the principal horizontal stress axes are rotating as one moves along the borehole. The trends are maintained for only a short distance before they reverse. The reversal points are almost always associated with the intersection of fractures and fracture zones with the boreholes, indicating that the rotations are related to stress perturbations localised at the fractures. Also, many DITFs either terminate or change their form (e.g. A-DITF becomes E-DITF) at natural fractures. So, definitively, natural fractures have a large influence on the variability of stress induced failure.

4.4.1 Characteristics of DITF Changes at Natural Fractures

At most intersections of DITFs with natural fractures, the DITF is unaffected and cuts through. However, in many cases, some change is seen. The types of terminations and transformations that DITFs generally undergo are shown in Figure 7 and their relative frequency of occurrence are shown in Figure 8a. About 70% of all observed DITFs either terminate or change from one form to the other (i.e. A-DITF to E-DITF) at natural fractures. Only 12–23% change from one form to the other remote from natural fractures. Of the remainder, 5–11% terminate remote from natural fractures, and a few stop near but not precisely at a natural fracture. In what follows we focus on the 70% that terminate or transform precisely at natural fractures since these suggest that the fractures are the source of the discontinuities in stress conditions at the borehole wall.

The types of change in DITFs that can occur at natural fractures are illustrated in Figure 7. Two types of E-DITFs are recognised according to whether they form in planes that are sub-parallel or oblique to the natural fracture. The relative frequency of occurrence of the various possible changes is shown in Figure 8b. Terminations of E-DITFs that are sub-parallel to the natural fractures are the most frequent in both wells, accounting for 41%, followed by termination of A-DITFs with 34–37%. Terminations of E-DITFs oblique to the natural fractures are rare. Of the transformations, only A-DITFs to E-DITFs that are sub-parallel to the fracture occur relatively frequently, the other two types being rare or non-existent. These changes for the

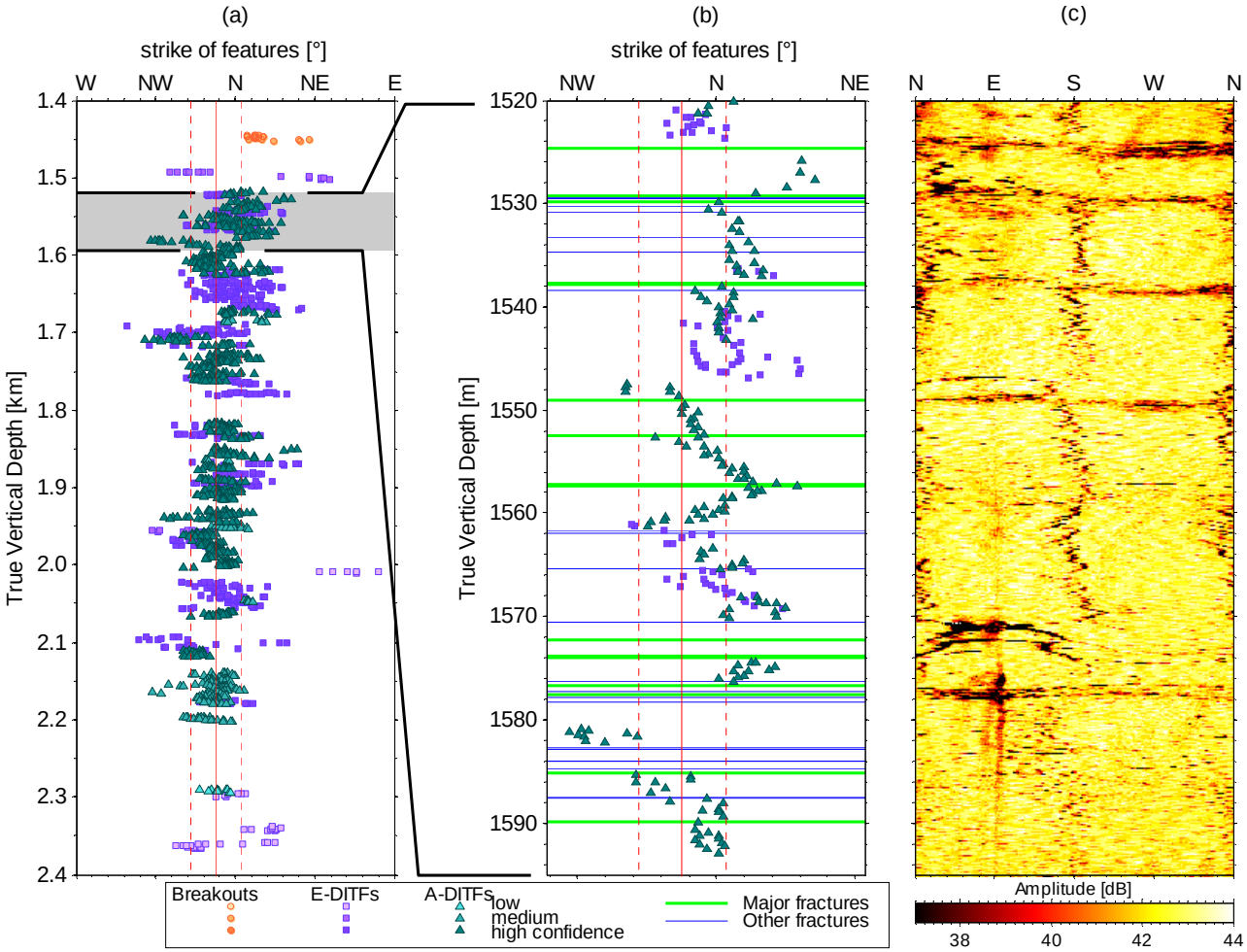

Figure 6: Expanded view (1520–1595 m TVD) of the variation of DITF strike in the upper granite sections of GPK4 illustrating the character of short wavelength (<50 m) variations. a) strike of A-DITFs (green triangles), E-DITFs(violet squares) and breakouts (orange circles) in the upper section of GPK4 with the latter rotated anticlockwise through 90° (see also figure 2). b) detailed view for the interval 1520 to 1595 m TVD including also location of natural fractures. c) Acoustic televiewer amplitude image for the same interval. The mean azimuth of SHmax and its standard deviation from all indicators in both GPK3 and GPK4 is denoted by the vertical redlines (N169°±14°) on a) and b).

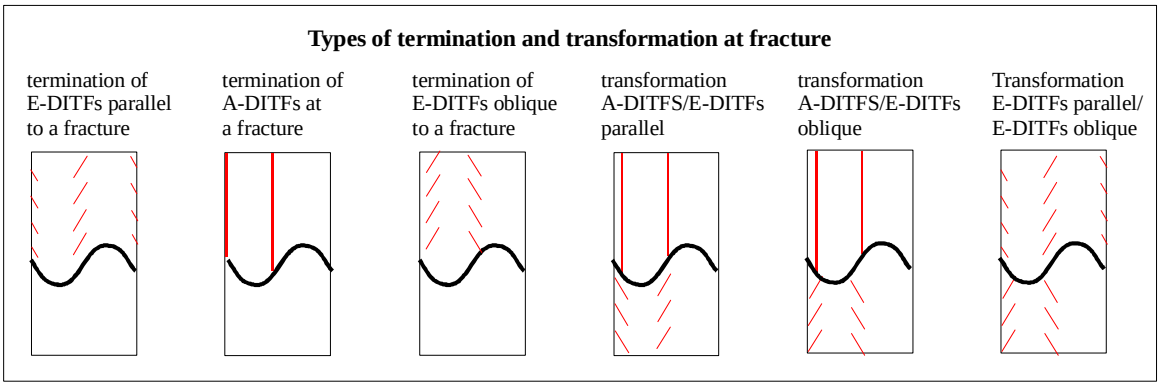

Figure 7: Types of terminations or transformation of DITF geometry that occur at natural fractures (see Figure 8b for relative frequency of occurrence).

most part indicate discontinuities in stress along the borehole wall that occur at natural fractures. Whilst the well-known tendency for natural fractures to arrest the propagation of tensile fractures might be a factor for some cases of termination, a change in either stress conditions or rock tensile strength on either side of the natural fracture must be present since otherwise DITFs would form on each side because of identical conditions.

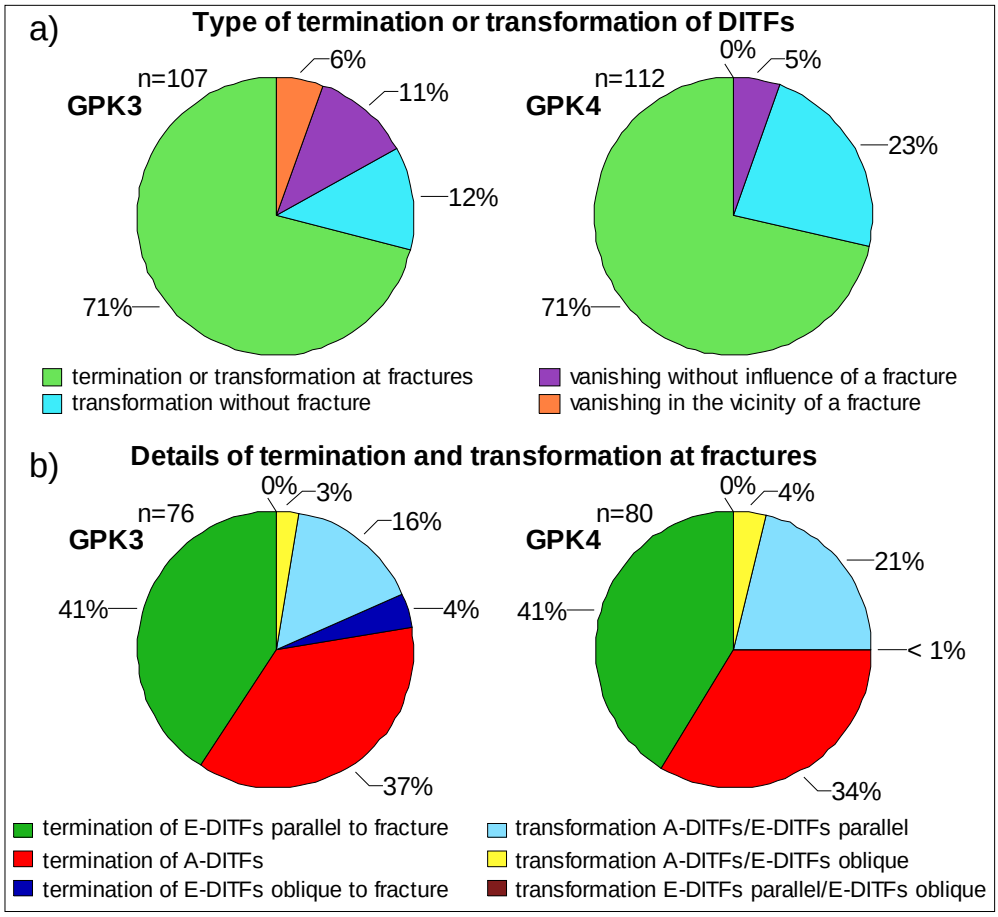

Figure 8: Terminations and transformations of DITFs. a) Relative frequency of types of termination or transformation of DITFs with regard to the proximity of natural fractures. b) Detail of the relative frequency of the types of terminations or transformation that occur at natural fractures (see Figure 7 for illustrations of the possible types).

4.4.2 Stress Perturbing Fractures

The preceding sections have served to establish the association of stress perturbations with natural fractures. In all, 144 fractures natural fractures in GPK4 could be unequivocally identified as associated with a stress perturbation through one of the following ways:

1. Orientation of induced failure (breakouts or DITFs) is modified in the vicinity of such fractures.

2. Induced failure stops on one side or the other of such fractures.

3. Induced failure changes form (i.e. A-DITFs to E-DITFs) in the vicinity of such fractures.

4. Induced failure is interrupted (i.e. no failure) in the vicinity of such fractures.

The 144 stress-perturbing fractures most surely underestimate the total number of stress-perturbing fractures since there are possibly many others that occur in regions of the borehole where conditions of wellbore failure were not met and thus there is no stress indicator generated in their vicinity. The distribution of the orientations of these fractures is shown in Figure 9a, together with the orientation distribution of all 2215 fractures identified in GPK4.

The orientations of stress-perturbing fractures are more closely distributed than the latter, and fall into two major families (272/78 and 080/66), which are also the dominant orientations for the complete dataset.

The effective normal and shear stress resolved on the stress-perturbing and complete fracture datasets under the linear stress characterization with ambient pore pressure are shown in the Mohr circle plots of Figure 9. All stresses have been normalized by the vertical stress, Sv. Evidently, almost all of the stress-perturbing fractures are critically-stressed in the sense that failure would occur of their strength were described by a Coulomb friction criterion with the coefficient of 0.6 (e.g. Barton et al., 1995; Evans, 2005; Ito and Zoback Mark, 2000; Zhang et al., 2002). As such, these fractures would be verging on failure under the simplified, linear representation of the prevailing stress field. The failure of these fractures will induce a stress perturbation, and thus the stress supported by these fractures will be modified from the values shown in Figure 9. The shear stress level supported by the fracture will be reduced, and this is particularly significant for fractures associated with sub-parallel E-DITFs. So it is possible that the perturbations in part reflect relatively recent failure associated with the on-going accommodation of crustal deformation (Zoback and Townend, 2001). However, it is also possible that they reflect failure that predates the contemporary stress situation.

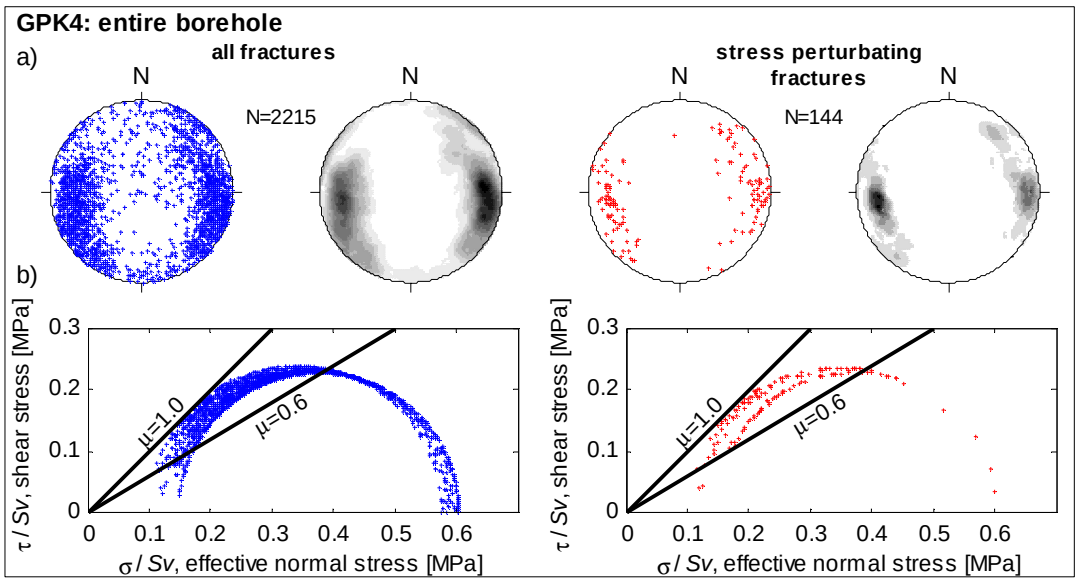

Figure 9: a) Stereographic plot of poles to all natural fractures identified in GPK4 (left) and the subset that were associated with stress perturbations (right). b) Mohr circle plots of the shear and effective normal stresses resolved on fracture sets in a). The stress was taken as given by the linear characterization for Soultz and the pore pressure as ambient.

5. CONCLUSIONS

Variations in the orientation of breakouts and DITFs about the mean orientations have been analyzed to investigate stress heterogeneity along the trajectory of the 5 km deep boreholes GPK3 and GPK4 at the Soultz site. The results suggest:

1) Variations in the stress orientation indicators occur at all scales amenable to analysis. Power spectra of the variations indicate power law behaviour between wavelengths 4 and 80 m, with slopes close to -2, indicative of self-affine behaviour. This indicates the relative amplitude of the variations with respect to wavelength decreases with larger scale.

2) The two most prominent large scale variations in horizontal principal stress orientation with wavelengths in excess of 100 m coincide with the two most significant fracture zones intersected by the wells. One of these occurs near 2000 m where the wells are only 20 m apart. Despite this lateral proximity, the large-scale variation is only partly correlated between wells, suggesting the presence of high lateral gradients in stress associated with the causal fracture zone.

3) Short-wavelength (<50m) variations in stress orientation with deviations from the mean of up to 90° occur frequently and are generally associated with natural fractures. Changes in stress across natural fractures are also indicated by coincident termination and transformation of DITFs from one form to another. Such variations are not usually correlated between wells in the section above 2000 m where the holes are 20 m apart

4) Almost all of the fractures which are associated with stress perturbations are critically stressed under the large-scale linear stress characterisation of the site. Thus, it is possible that they failed and generated the stress perturbations relatively recently, reflecting accommodation of on-going tectonic deformation of the crust. However, the data do not require this, and it is just as likely that the slip that generated the stress perturbations is much older.

6. AKNOWLEDGEMENTS

This work was supported by the Swiss State Secretariat for Education and Research under project number 03.04.60, and was performed as a contribution to the European Union's FP6 project 'Soultz EGS Pilot Plant' funded by ADEME, BMU, EC and EEIG 'Exploitation Minière de la Chaleur'. We thank EEIG for access to the data, and Albert Genter, Marion Pfender and Dimitra Teza for helpful information.

REFERENCES

Anders, M. H., and D. V. Wiltschko (1994), Microfracturing, paleostress and the growth of faults, *Journal of Structural Geology*, *16*, 795-815.

Barton, C. A., and M. D. Zoback (1994), Stress perturbations associated with active faults penetrated by boreholes: Possible evidence for near-complete stress drop and a new technique for stress magnitude measurements, *Journal of Geophysical Research*, *99*, 9373-9390.

Barton, C.A., Zoback, M.D. & Moos, D., 1995. Fluid flow along potentially active faults in crystalline rock, *Geology*, 23**,** 683-686.

Bell, J. S., and D. I. Gough (1979), Northeast-southwest compressive stress in Alberta: Evidence from oil wells, *Earth and Planetary Science Letters*, *45*, 475-482.

Bérard, T. (2003), Estimation du champ de contrainte dans le massif granitique de Soultz-sous-Forêts, implication sur la rhéologie de la croûte fragile, 264 pp, Institut de Physique du Globe de Paris, Paris.

Cornet, F. H., et al. (1992), Stress Heterogeneities and Flow Paths in a granite Rock Mass, Pre-Workshop Volume for the Workshop on Induced Seismicity, paper presented at 33rd U.S. Symposium on Rock Mechanics 184.

Cornet, F. H., and Y. Jianmin (1995), Analysis of induced seismicity for stress field determination and pore pressure mapping, *Pure and Applied Geophysics*, *145*, 677-700.

Cornet, F. H., et al. (2007), How close to failure is natural granite rock mass at 5 km depth ?, *International Journal of Rock Mechanics and Mining Sciences*, *44*, 47-66.

Cowie, P. A., and C. H. Scholz (1992), Physical explanation for the displacement-length relationship of faults using a post-yield fracture mechanics model, *Journal of Structural Geology*, *14*, 1133-1148.

Cuenot, N., et al. (2006), Faulting mechanisms and stress regime at the European HDR site of Soultz-sous-Forets, France, *Geothermics*, *35*, 561-575.

Dezayes, C., et al. (2004), Fracture network of the EGS geothermal reservoir at Soultz-sous-Forêts (Rhine graben, France), in *Geothermal Research Council 2004*, edited.

Dezayes, C., et al. (2010), Overview of the fracture network at different scales within the granite reservoir of the EGS Soultz site (Alsace, France). Proceedings World Geothermal Congress 2010 Bali, Indonesia, 25-29 April 2010

Dorbath, L., and J. Charléty (2007), What can we learn from large induced earthquakes at Soultz-sous-Forêts, paper presented at EHDRA scientific conference, 28 - 29 June 2007, Soultz-sous-Forêts, France, 28-29 June 2007.

Evans, K. F. (2005), Permeability creation and damage due to massive fluid injections into granite at 3.5 km at Soultz: 2. Critical stress and fracture strength, *Journal of Geophysical Research*, *110*.

Faulkner, D. R., et al. (2006), Slip on 'weak' faults by the rotation of regional stress in the fracture damage zone, *Nature*, *444*, 922-925.

Harris, R. A. (1998), Introduction to special section: Stress triggers, stress shadows, and implications for seismic hazard, *Journal of Geophysical Research*, *103*, 24347-24358.

Hettkamp, T., et al. (2004), Electricity production from hot rocks, paper presented at 29th workshop on geothermal reservoir engineering, Stanford, 26-28 January 2004.

Ito, T. & Zoback, M.D., 2000. Fracture permeability and in situ stress to 7 km depth in the KTB Scientific Drillhole, *Geophysical Research Letters*, 27**,** 1045-1048.

Ito, T., et al. (2001), Utilization of Mud Weights in Excess of the Least Principal Stress to Stabilize Wellbores: Theory and Practical Examples, *SPE Drilling and Completion*, *16*, 221-229.

Kastrup, U., et al. (2004), Stress field variations in the Swiss Alps and the northern Alpine foreland derived from inversion of fault plane solutions, *Journal of Geophysical Research*, *109*.

Mastin, L. (1988), Effect of borehole deviation on breakout orientations, *journal of Geophysical Research*, *93*, 9187-9195.

Peška, P., and M. D. Zoback (1995), Compressive and tensile failure of inlclined well bores and determination of in situ stress and rock strength, *Journal of Geophysical Research*, *100*, 12791-12811.

Power, W. L., and T. E. Tullis (1991), Euclidian and Fractal Models for the Description of Rock Surface Roughness, *Journal of Geophysical Research*, *61*, 415-424.

Rice, J. R. (1992), Fault stress states, pore pressure distributions, and the weakness of the San Andreas Fault., in *Fault mechanics and transport properties of rocks*, edited by B. Evans and T.-F. Wong, pp. 475-503, Academic Press, London.

Sausse, J., et al. (2007), From geological interpretation and 3D modelling of the characterization of the deep seated EGS reservoir of Soultz (France), paper presented at EHDRA scientific conference, 28 - 29 June 2007, Soultz-sous-Forêts, France, 28 and 29 June 2007.

Scotti, O., and F. H. Cornet (1994), In-situ stress fields and focal mechanism solutions in central France, *Geophysical Research Letters*, *21*, 2345-2348.

Shamir, G. (1990), Crustal stress orientation profile to a depth of 3.5 km near the San Andreas Fault at Cajon Pass, California Stanford University.--Dept. of Applied Earth, Sciences.

Shaw, B. E. (2004), Dynamic heterogeneities versus fixed heterogeneities in earthquake models, *Geophysical Journal International*, *156*, 275-286.

Stanchits, S., et al. (2006), Ultrasonic Velocities, Acoustic Emission Characteristics and Crack Damage of Basalt and Granite, *Pure and Applied Geophysics*, *163*, 975-994.

Stoica, P., and R. L. Moses (1997), *Introduction to Spectral Analysis*, 319 pp., Prentice-Hall.

Thompson, B., et al. (2006), Fracture in Westerly Granite under AE Feedback and Constant Strain Rate Loading: Nucleation, Quasi-static Propagation, and the Transition to Unstable Fracture Propagation, *Pure and Applied Geophysics*.

Tischner, T., et al. (2007), HDR project Soultz: hydraulic and seismic observations during stimulation of the 3 deep wells by massive water injections, in *32nd Workshop on Geothermal Reservoir Engineering*, edited, Stanford, California.

Turcotte, D. L. (1989), Fractals in geology and geophysics, *Pure and Applied Geophysics*, *131*, 171-196.

Valley, B., 2007. The relation between natural fracturing and stress heterogeneities in deep-seated crystalline rocks at Soultz-sous-Forêts (France), PhD, Eidgenössische Technische Hochschule ETH Zürich, Nr. 17385

Valley, B., and K. F. Evans (2007), Stress state at Soultz-sous-Forêts to 5 km depth from wellbore failure and hydraulic observations, paper presented at 32nd workshop on geothermal reservoir engineering, Stanford, 22-24 January 2007.

Vermilye, J. M., and C. H. Scholz (1998), The process zone: A microstructural view of fault growth, *Journal of Geophysical Research*, *103*, 12223-12238.

Wilson, J.E., Chester, J.S. & Chester, F.M., 2003. Microfracture analysis of fault growth and wear processes, Punchbowl Fault, San Andreas system, California, *Journal of Structural Geology*, 25**,** 1855-1873.

Zhang, X., Sanderson, D.J. & Barker, A.J., 2002. Stress control of hydraulic conductivity in fracture-saturated Swedish bedrock, *Geophysical Journal International*, 151**,** 452-468.

Zoback, M. D., et al. (1987), New Evidence on the State of Stress of the San Andreas Fault System, *Science*, *238*, 1105-1111.

Zoback, M.D. & Townend, J., 2001. Implications of hydrostatic pore pressures and high crustal strength for the deformation of intraplate lithosphere, *Tectonophysics*, 336**,** 19-30.

Zoback, M. D., et al. (2003), Determination of stress orientation and magnitude in deep wells, *International Journal of Rock Mechanics and Mining Sciences*, *40*, 1049-1076.

Zöller, G., et al. (2005), The Role of Heterogeneities as a Tuning Parameter of Earthquake Dynamics, *Pure and Applied Geophysics*, *162*, 1027-1049.